BILINGUAL PUBLISHING CO.
*Advances in Modern Oncology Research*
doi: 10.30564/amor.v5i2.235

Article

# Targeted Graphene Oxide for Integrated Tumor Diagnosis and Treatment

**Jinghuan Zhang***
Oncology Research Society, China

***Correspondence Author:** Jinghuan Zhang, Oncology Research Society, China; Email: zhangjh@163.com

***Abstract:*** Integrin αvβ3 (V3) is a typical tumor marker, which provides a basis for the diagnosis of tumor types and also provides potential target for tumor treatment. The chemical nature of V3 is a transmembrane glycoprotein, which is highly expressed on the surface of a variety of tumor cells, such as human malignant glioma (U87-MG). Therefore, the study used U87-MG cells as the treatment model, using V3 monoclonal antibody (V3MA) as the most targeted ligand, coupled with a novel nano-graphene oxide (NGO) as a photothermal agent. A new type of nanoprobe (NGO-mAb-FITC) was constructed for targeted imaging and photothermal therapy of tumor. The nanoprobe has the active targeting effect of recognizing U87-MG of V3-positive cells, but cannot recognize human breast cancer cells (McF-7) with negative expression of V3. By covalently modifying target ligands with fluorescein isothiocyanate (FITC), nanoprobes (NGO-mAb-FITC) can achieve targeted imaging effects on tumor cells. Meanwhile, the photothermal transformation of GO under 805 nm near-infrared (NIR) light enabled tumor cells to specifically absorb NGO-mAb-FITC nanoprobe and realize hyperthermia, thus inducing thermal damage and cell apoptosis. The results showed that NGO-mAb-FITC could effectively identify V3-positive tumor cells and provide evidence for tumor diagnosis. The high photothermal conversion ability of GO provides a new approach for tumor therapy, and GO is expected to be a potential new targeted photothermal conversion probe for tumor imaging diagnosis and photothermal therapy.

***Keywords:*** Targeted imaging; Photothermal therapy; Nano-grapheneoxide

***Received:*** 21 February 2019; ***Accepted:*** 6 March 2019; ***Published Online:*** 1 April 2019

## 1. Introduction

Cancer has become the main cause of death from diseases worldwide. The development of early diagnosis and treatment technologies for cancer is the key to ensuring public health, and it is also a current research hotspot in the field of medicine and pharmacy. Early diagnosis of cancer is of great significance to improve the survival rate and cure rate of tumor patients [1-2]. With the rapid development of nanotechnology, biopharmaceutical and other fields, nanotechnology has changed the pattern of biomedicine. Molecular diagnostics and molecular imaging technologies developed based on nanotechnology are increasingly being applied to early diagnosis of tumors [3-4]. For example, Hwang et al. reported the multifunctional nanoprobe MF-AS1411 that can efficiently target rat glioma cells overexpressing nucleolin, and the nanoprobe has been successfully used to tumor imaging diagnosis in mice [5]. High-resolution deep tissue optical imaging technology is playing an increasingly important role in the field of biomedical imaging. However, problems such as strong light scattering and tissue penetration limit its application in the light transmission path in biological tissues and *in vivo* imaging [6]. Wang et al. developed the X-ray tomographic imaging technology using functionalized nano-probe AuNR1000-EGFR as an exogenous PAT (photoacoustictomography) contrast agent to provide another high-resolution imaging diagnostic method for tumor diagnosis. Among them, EGFR was a targeting ligand, and the essence of this targeting ligand was a tumor marker [7]. Tumor markers refer to substances that

are characteristically present in malignant tumor cells, or are abnormally produced by malignant tumor cells, or are produced by the host's response to tumor stimulation. The tumor maker can reflect tumor occurrence and development, and monitor tumor response to treatment [8]. Conventional tumor imaging technologies mostly use tumor markers to distinguish tumor cells from normal cells. The tumor markers are installed on the surface of nanocarriers through covalent modification or non-covalent modification, and they are specifically targeted for tumor cells, and the functionalized nanoprobes are used for molecular imaging of tumors [9]. Under certain light excitation, the nanoprobe can generate electron transition, thus producing strong fluorescence for imaging, such as silkworm quantum dots, carbon nanotubes, gold nanorods and graphene [10-14].

Graphene is a hexagonal honeycomb lattice plane film composed of carbon atoms with sp2 hybrid orbitals. It has a large specific surface area and excellent electrical, mechanical, optical, and thermal ability [15-17]. It is known as the best carbon materials with development potential in the 21st century. GO has good absorption in the NIR region, and there are more functional groups in the surface of GO, so that it can be uniformly dispersed in water. GO has the advantages of large specific surface area, low cytotoxicity, and low production cost, which can be used as a new type of biocompatible nanomaterials applied in the field of biomedicine [18-19].

Based on the unique photothermal conversion performance of GO, we developed a new type of nanoprobe (NGO-mAb-FITC), in which the V3MA was used as the targeting ligand, and it was easily soluble in water and interacted with protein. The strong binding force of FITC isomer type I was a fluorescent marker [20-21]. The new type of nanoprobe has high affinity for tumor cells, which can be used in imaging of tumors. In addition, the excellent photothermal conversion performance of GO under near-infrared laser irradiation at 805nm mediated photothermal therapy, which can kill tumor cells effectively [22].

## 2. Materials and Methods

### 2.1 Materials

CCK-8 was available at Dojindolabor-atories (Kumamoto Prefecture, Japan). NGO (Nanjing Pioneer Nanotechnology Co., LTD.), N-hydroxysuccinimide (NHS), E1-ethyl-3 -(3-dimethylaminopropyl) carbodiimide (EDC) and FITC were purchased from Sigma.

### 2.2 Synthesis and Characterization of Materials

2 mL of NGO aqueous solution (pH 7.4, 2 mg/mL) were centrifuged (5000 r/min) for 10 min, taking the supernatant to remove the precipitate. 500 μL of 0.1 mol/L concentrated hydrochloric acid (HCl) were added dropwise in the solution. The above solution were reacted with concentrated HCl for 4 h in the ultrasonic machine, then washing with deionized water. And then the solution were centrifuged at 10000 r/min for 10 min to remove HCl, repeated 5 times. 0.1 mol/L sodium acetate was added to the above substances, and the reaction was sonicated again for 4 h. Then the sodium acetate was removed by centrifugation at 10 000 r/min for 10 min, and washing with deionized water and centrifuging at 10,000 r/min for 10 min, repeated 5 times. Finally, phosphate buffer solution (PBS, pH7.4) was used for resuspenting, and the final concentration was 2 mg/mL. The resulting carboxylated NGO (NGO-COOH) was tested using the raman spectra.

### 2.3 Synthesis of Nanoprobe

First, 500μL of NGO-COOH (2mg/mL) were added to the 1.5mL EP tube, and then 300μL of 6μg/mL mAb-FITC (covalently linking the V3MA with the fluorescent dye FITC through an amide bond) were added. Subsequently, 100 μL of 100 mmol/L EDC and 100 μL of 50 mmol/L NHS solution were added to the EP tube, stirred at room temperature for 8 hours, and centrifuging at 10 000 r/min for 10 minutes to remove excess mAb-FITC. The obtained sample was washed with deionized water, repeated 5 times. Finally, PBS (pH7.4) was used for resuspenting, and the final concentration was 2 mg/mL. The nanoprobe NGO-mAb-FITC was detected by ultraviolet-visible (UV-vis) spectrophotometer, fluorescence spectrometer and atomic force microscope (AFM).

### 2.4 Photothermal Conversion Ability

1 mL of NGO-mAb-FITC (1~2mg/mL) was added to a 1.5mL EP tube, and then irradiating for 5 minutes at a 805nm laser power with 1~2W/cm$^2$. An infrared thermal imager was used to record the changes of temperature every minute.

### 2.5 Anti-tumor Effect *in vitro*

U87-Mg cells and MCF-7 cells were placed in 1640 medium containing 10% MEM, and cultured in an incubator containing 5% $CO_2$ at 37 °C. The U87-Mg cells and MCF-7 cells were planted in a 2×2 cell culture dish ($10^4$/mL) for overnight. 500μL of a mixture of fresh culture medium and nanoprobe NGO-mAb-FITC (9:1) were add-


10.30564/amor.v5i2.235

ed in the dish, incubating for 3 hours in the dark. The cells were washed with 37°C PBS buffer (pH 7.4) 3 times to remove the free NGO-mAb-FITC. Finally, fresh culture medium were added for 30min incubation, and putting the cells into the sample tank of the confocal microscope for observation.

U87-MG cells were cultured in a 96-well plate with $10^4$ cells in each well. 100 L of MEM medium containing 10% FBS was added and cultured overnight. Then 20 L NGO-mAb-FITC (25~100 g/mL) were added for 3h, then washed with PBS buffer for 3-2 times. The 805nm laser was turned on (1.5w /$cm^2$, 5min) to irradiate cells. Then 100 μL of fresh culture medium was added for 24h. Then the culture medium was removed, and the mixture of culture medium and CCK-8 reagent was configured in a 9:1 ratio to keep the total volume at 100 μL.

## 3. Results and Discussion

### 3.1 Characterization of Materials

NGO is a two-dimensional crystalline nanomaterial. In the sp2 hybrid orbital domain, monolayer atomic layers are arranged in a honeycomb lattice [23]. However, due to the intervention of strong oxidant, the surface carbon skeleton structure was destroyed and sp3 hybridized carbon atoms were formed on the surface in synthetic process (Figure 1). As shown in Figure 2, after oxidation of HCl (1 mol/L) and water bath ultrasound treatment with 1 g sodium acetate, the raman spectrum of NGO was detected, which showed that the NGO had two peaks around 1340.5 $cm^{-1}$(D peak) and 1585.2 $cm^{-1}$ (G peak). By analyzing the cause of formation, we speculated that the introduction of the oxygen-containing group destroyed the carbon sp2 hybridization orbit on the surface of the original graphene, and then formed sp3 hybridized carbon atoms, which showed a wide D-peak shape. While the vibration of sp2 hybridized carbon atoms represented by sp2 and G peak was an inherent characteristic peak of graphite crystal materials. NGO had hydroxyl groups, carboxyl groups and other oxygen-containing groups on its surface and edges, and the presence of oxygen-containing groups made it easy to be covalently coupled with V3MA. Subsequently, the NGO-COOH was reacted with NHS for 30min to activate the carboxyl group, providing higher activation energy for further coupling with MAB-FITC via amide bond. After the reaction, EDC was added for amide condensation reaction for 6~12 h, and NGO-mAb-FITC were finally obtained. To prove that NGO and mAb-FITC were successfully connected, the absorption spectrum and fluorescence spectrum of NGO-mAb-FITC and NGO were tested respectively. As shown in Figure 3a, the absorption spectrum of NGO-mAb-FITC was caused by the superposition of NGO and mAb-FITC. In the fluorescence spectrum, mAb-FITC had a characteristic emission peak at about 520 nm by excitation light of 488 nm, but NGO had a high fluorescence quenching effect on FITC dye. As shown in Figure 3b, the NGO had quenching effect on MAB-FITC, indicating that MAB-FITC has successfully conjugated to the surface of NGO. In order to further understand the scale of the nanoprobe, AFM was used for detection of modified morphology characteristics. As shown in Figure 4, the size of NGO-mAb-FITC probe was ~500 nm, and white particles attached to the surface of NGO-mAb-FITC material can be clearly observed in the image. The white particles were mAb-FITC, suggesting that mAb-FITC covalently band to NGO via amide bond.

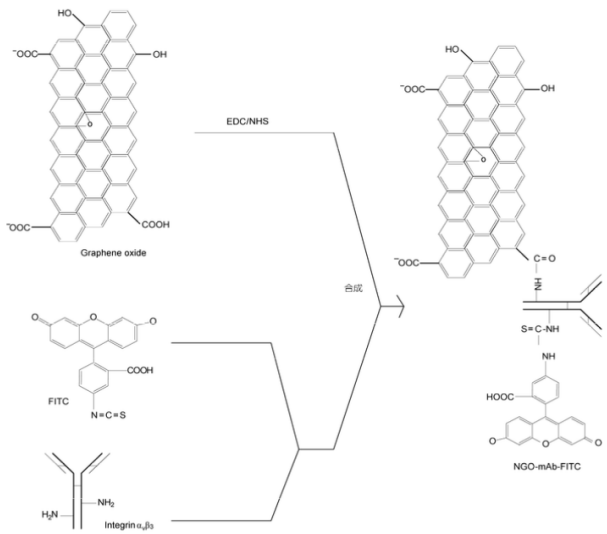


**Figure 1.** Flow chart of nanoprobe NGO-mAb-FITC construction

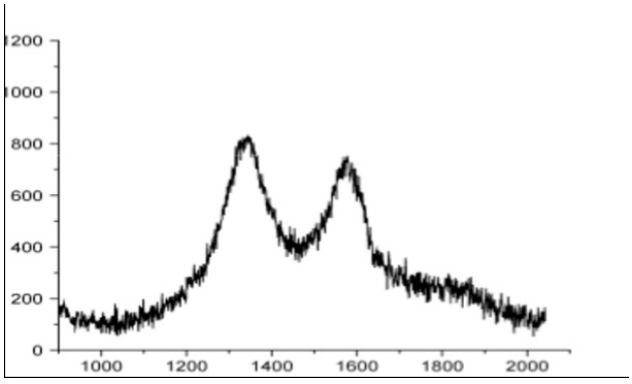


**Figure 2.** Raman spectroscopy of NGO

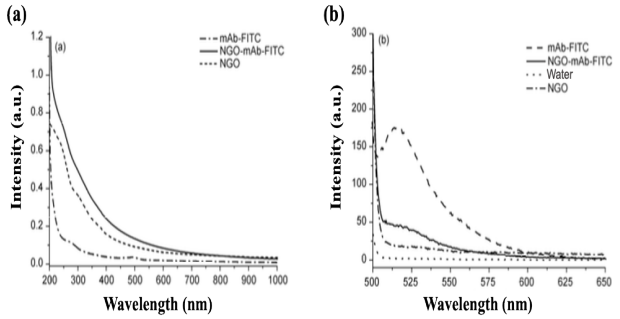


**Figure 3.** (a) Absorption spectra and (b) fluorescence spectra of NGO, NGO-mAb-FITC, water and mAb-FITC

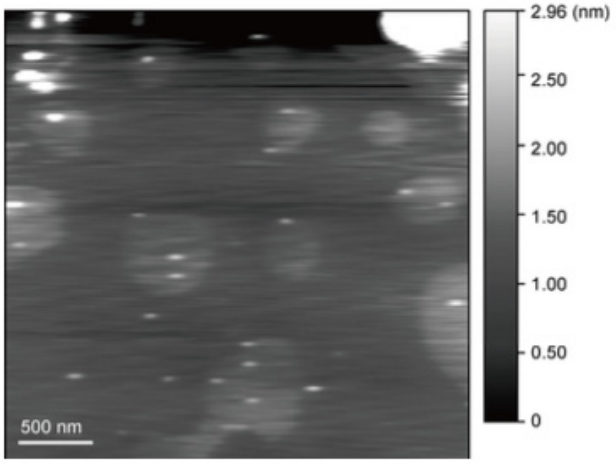


**Figure 4.** The AFM image of NGO-mAb-FITC

## 3.2 Targeted Imaging of Specific Tumor Cells

V3 was highly expressed on the surface of U87-MG cells, but not on the surface of MCF-7 cells. Therefore, U87-MG cells and MCF-7 cells were treated with nanoprobe respectively, and then the confocal microscopy was used to observe the cell imaging. As shown in Figure 5, compared with the control group (a) and (b), U87-MG cells showed stronger fluorescence than that of (c) and (e). However, the MCF-7 cells showed no fluorescence (d) and (f), and the fluorescence in U87-MG cells increased with the increase of NGO-mAb-FITC concentration, which was due to that the difference between the two cell lines was the express of V3. The results demonstrated that NGO-mAb-FITC nanoprobe was able to target U87-MG with high expression of V3 on the surface through antigen-antibody interaction, and nanoprobe was highly absorbed by the tumor cells for the purpose of targeted localization imaging and diagnosis. However, the MCF-7 cells were not recognized by the nanoprobe, which further confirmed the high selectivity of the NGO-mAb-FITC nanoprobe constructed.

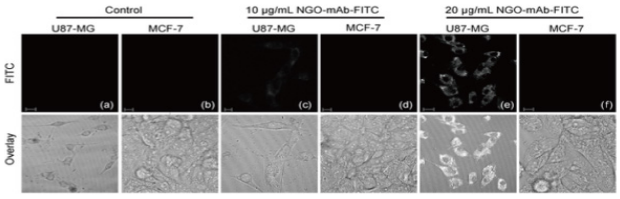


**Figure 5.** The targeted imaging of U87-MG cells and MCF-7 cells treated with different concentration of NGO-mAb-FITC for 3h

## 3.3 Photothermal Conversion Ability

The above experiments confirmed that NGO-mAb-FITC nanoprobe could efficiently target U87-MG cells, while NGO could reach local high temperature in a relatively short time under NIR light irradiation of 805 nm, which was speculated that this property could be further used for thermal killing of tumor cells. Therefore, the photothermal performance detection experiment of NGO-mAb-FITC nanoprobe was carried out. The photothermal conversion curves of NGG-mAb-FITC nanoprobe with the same power density and different concentrations were showed in Figure 6a. The results showed that under the same power density, the NGO-mAb-FITC nanoprobe with 2 mg/mL had the strongest photothermal conversion ability and the temperature was up to 55°C, and the temperatures of the nanoprobe could increase with the increase of the concentration of NGO-mAb-FITC nanoprobe. Figure 6b showed that the temperatures of NGO-Mab-FITC increased with the increase of power density, which suggested that the local excessive heat generated by NGO-mAb-FITC nanoprobe would have a potential on photothermal therapy.

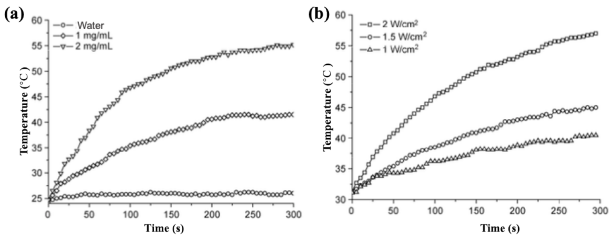


**Figure 6.** (a) Photothermal curves of nanoprobe with different concentrations over time. (b) Photothermal curves of nanoprobe irradiated by different power laser over time

## 3.4 Anti-tumor Effect

CCK-8 experiment was conducted to investigate the effect of nanoprobe on the proliferation activity of U87-MG cells to reflect the photothermal effect of nanoprobe on tumor cells. As shown in Figure 7, under the irradiation of NIR laser (1.5 W/cm$^2$, 5 min), NGO-

mAb-FITC nanoprobe had the great influence on the proliferation activity of cocultivation U87-MG cells. Under the same light conditions, the effect of NGO-mAb-FITC on the proliferation rate of U87-MG cells was concentration-dependent. The results indicated that due to the increased concentration, NGO-mAb-FITC photothermal conversion produced higher heat, which could effectively kill tumor cells and serve as the purpose of tumor therapy.

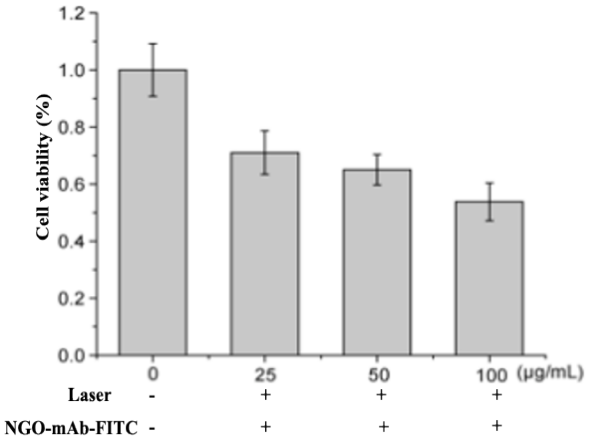


**Figure 7.** Anti-tumor effect by NGO-mAb-FITC

## 4. Conclusion

In this study, a novel NGO functional nanoparticle probe NGO-mAb-FITC was constructed. V3MA can effectively target U87-MG and realize fluorescence imaging diagnosis of these cells by detecting fluorescence of FITC. Due to the large number of functional groups (such as carboxyl and hydroxyl groups) on the surface of NGO, it was easy to connect biological macromolecules such as monoclonal antibodies and polypeptides. The design procedure of this scheme is simple and feasible, which can replace the corresponding targeted ligands for different types of tumor cells and achieve the purpose of imaging diagnosis for different types of tumors. In addition, NGO had strong photothermal conversion performance under 805nm NIR laser, which can cause local overheating of target cells and effectively inhibit tumor growth. The local temperature in the tumor area is higher than that of the normal tissue cells, which can be further used for photothermal imaging in the tumor area. The study provides the possibility for further tumor targeted imaging diagnosis and treatment.

## References

[1] Argiris K, Panethymitaki C, Tavassoli M. Naturally occurring, tumor-specific, therapeutic proteins. Exp Biol Med (Maywood), 2011, 236: 524-536.

[2] Bleyer A. Cancer of the oral cavity and pharynx in young females: Increasing incidence, role of human papilloma virus, and lack of sur- vival improvement. Semin Oncol, 2009, 36: 451-459.

[3] Okura H. Usefulness of tumor marker in early diagnosis. Nihon Naika Gakkai Zasshi, 2005, 94: 2479-2485.

[4].Xiang L, Yuan Y, Xing D, et al. Photoacoustic molecular imaging with antibody-functionalized single-walled carbon nanotubes for early diagnosis of tumor. J Biomed Opt, 2009, 14: 021008.

[5] Hwang D W, Ko H Y, Lee J H, et al. A nucleolin-targeted multimodal nanoparticle imaging probe for tracking cancer cells using an ap- tamer. J Nucl Med, 2010, 51: 98-105.

[6] Kim C, Favazza C, Wang L V. In vivo photoacoustic tomography of chemicals: High-resolution functional and molecular optical imaging at new depths. Chem Rev, 2011, 110: 2756-2782.

[7] Lamerz R. Role of tumour markers, cytogenetics. Ann Oncol, 1999, 10(Suppl 4): 145-149.

[8] Amayo A A, Kuria J G. Clinical application of tumour markers: A review. East Afr Med J, 2009, 86: S76-S83.

[9] Berlin J M, Pham T T, Sano D, et al. Noncovalent functionalization of carbon nanovectors with an antibody enables targeted drug delivery.ACS Nano, 2011, 5: 6643-6650.

[10] Sun X, Liu Z, Welsher K, et al. Nano-graphene oxide for cellular imaging and drug delivery. Nano Res, 2008, 1: 203-212.

[11] Cho H S, Dong Z, Pauletti G M, et al. Fluorescent, superparamagnetic nanospheres for drug storage, targeting, and imaging: A multifunc-tional nanocarrier system for cancer diagnosis and treatment. ACS Nano, 2010, 4: 5398-5404.

[12] Chen J, Chen S, Zhao X, et al. Functionalized single-walled carbon nanotubes as rationally designed vehicles for tumor-targeted drug de-livery. J Am Chem Soc, 2008, 130: 16778-16785.

[13] De la Zerda A, Liu Z, Bodapati S, et al. Ultrahigh sensitivity carbon nanotube agents for photoacoustic molecular imaging in living mice.Nano Lett, 2010, 10: 2168-2172.

[14] Kim J W, Galanzha E I, Shashkov E V, et al. Golden carbon nanotubes as multimodal photoacoustic and photothermal high-contrast mo-lecular agents. Nat Nanotech, 2009, 4: 688-694.

[15] Yang K, Zhang S, Zhang G, et al. Graphene in mice: Ultrahigh in vivo tumor uptake and efficient photothermal therapy. Nano Lett, 2010, 10: 3318-3323.

[16] Kalkanidis M, Pietersz G A, Xiang S D, et al. Methods for nano-particle based vaccine formulation and evaluation of their immunogenic-ity. Methods, 2006, 40: 20-29.

[17] Dresselhaus M S, Araujo P T. Perspectives on the 2010 Nobel Prize in physics for graphene. ACS Nano, 2010, 4: 6297-6302.

[18] Wang Y, Jaiswal M, Lin M, et al. Electronic properties of nanodiamond decorated graphene. ACS Nano, 2012, 6: 1018-1025.

[19] Markovic Z M, Harhaji-Trajkovic L M, Todorovic-Markovic B M, et al. In vitro comparison of the photothermal anticancer activity of graphene nanoparticles and carbon nanotubes. Biomaterials, 2011, 32: 1121-1129.

[20] Englert J M, Dotzer C, Yang G, et al. Covalent bulk functionalization of graphene. Nat Chem, 2011, 3: 279-286.

[21] Buonaguro L, Petrizzo A, Tornesello M L, et al. Translating tumor antigens into cancer vaccines. Clin Vaccine Immunol, 2011, 18: 23-34.

[22] Wang L, Zhao J, Sun Y Y, et al. Characteristics of Raman spectra for graphene oxide from ab initio simulations. J Chem Phys, 2011, 135:184503.

[23] Zharv V P. Photothermal imaging of nanoparticles and cells. IEEE J Select Topic Quant Electron, 2005, 11: 733-751.



10.30564/amor.v5i2.235